Original article

Nanofluid impact on fluid interaction and migration characteristics for enhanced oil recovery in Baikouquan tight glutenite

Xiaomin Cao[1,2], Qi Li[1,2]*, Matthew Myers[3], Liang Xu[1,2], Quan Chen[1,2], Yongsheng Tan[1,2]

[1]*State Key Laboratory of Geomechanics and Geotechnical Engineering, Institute of Rock and Soil Mechanics, Chinese Academy of Sciences, Wuhan 430071, P. R. China*

[2]*University of Chinese Academy of Sciences, Beijing 100049, P. R. China*

[3]*CSIRO Energy, Australian Resources Research Centre, 26 Dick Perry Avenue, Kensington, Western Australia 6151, Australia*

Abstract:
Nanofluids have broad prospects in enhancing the oil recovery of reservoirs with low porosity, low permeability, high capillary pressure and low oil recovery. However, the modification effects of nanofluids on tight glutenite reservoirs remain unknown. In this paper, nanofluids with different proportions of silica nanoparticles and sodium dodecyl sulfate were prepared and characterized by zeta potential and particle size distribution. Then, the effects of nanofluids on interfacial tension and reservoir wettability were examined. Next, a computational fluid dynamics method was adopted to further investigate the effects of nanofluids and injection pressure on enhancing oil recovery of the Baikouquan Formation at the pore scale. The experimental results showed that all prepared nanofluids are stable systems with uniform dispersion. The interfacial tension between the nanofluids and oil was reduced by up to 8.01% compared with water, and the reservoir wettability was changed from intermediate-wet to strong hydrophilicity. The simulation results revealed that the water and nanofluid flooding processes could be divided into two stages: the initial channel establishment stage and the channel expansion stage. In the initial stage, the nanofluids hardly showed an enhanced oil recovery effect due to the faster and sharper migration fronts. In the channel expansion stage, the nanofluids clearly showed an enhanced oil recovery effect, as the nanofluids could displace the oil in the relative dead pores during water flooding. After 10 pore volume injection of displacement fluid at an injection pressure of 1 MPa, the oil recovery using NF5 was highest at 76.58%. In addition, a higher injection pressure led to the extraction of relative dead oil at a lower injection pressure near the inlet with a smaller sweep area near the outlet; the effect on recovery has both advantages and disadvantages.

1. Introduction

China, as the world's second largest economy, heavily relies on oil imports due to a deficiency in domestic oil production with external dependence on crude oil reaching 71.3% in 2022 (Wang et al., 2023). The increasing global demand for crude oil has led to a significant energy gap that is predicted to remain for at least the next two decades, despite the transition away from fossil fuels (Bera et al., 2021; Rashidi et al., 2021; Chowdhury et al., 2022). It is estimated that only approximately one-third of oil in a reservoir could be produced through primary and secondary methods in current oil production technology and geological conditions (Kalam et al., 2021; Mmbuji et al., 2021); thus, exploiting the residual oil in reservoirs is necessary (Sidiq et al., 2019). The Mahu oilfield is located at the northwestern margin of the Junggar Basin in Northwest China (Fig. 1), which is the largest tight glutenite oilfield in the world. The Triassic Baikouquan
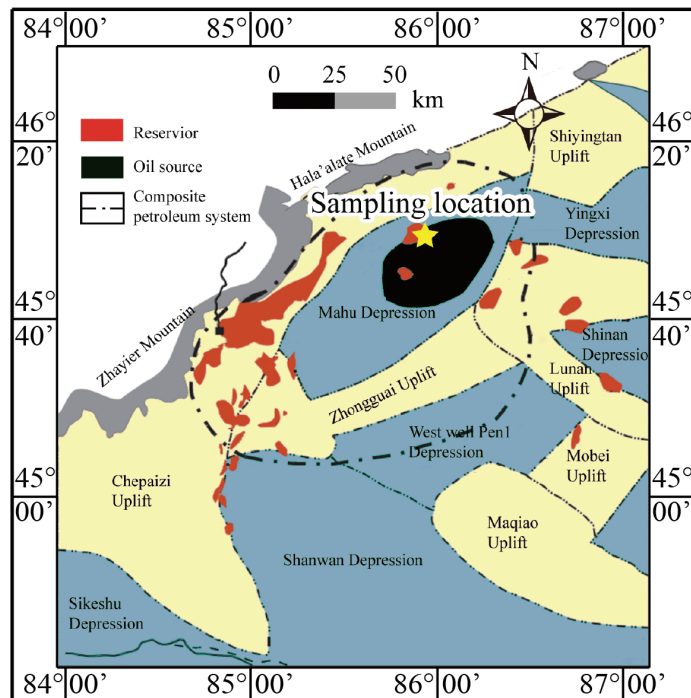
Fig. 1. Sampling location in the Mahu depression of Junggar Basin, Northwest China.

Formation, a fan delta sedimentary system is the main oil layer inside the Mahu oilfield reservoir. The distribution of the Baikouquan Formation is generally stable, with a total thickness between 112 and 173 m and an average thickness of 135 m. The reservoir lithology of the Baikouquan Formation is mainly composed of gray sandy glutenite, coarse sandstone and sandy glutenite. X-ray diffraction results show that the main mineral compositions are quartz (44.92%), potassium feldspar (14.53%), plagioclase (30.39%), calcite (6.61%) and montmorillonite (3.55%). The average porosity, permeability and capillary radius are 8.80%, 1.43 mD and 0.54 μm, respectively. After perforation, there was almost no oil production in the Baikouquan Formation due to the elasticity of the reservoir itself. In addition, preliminary tests showed that water flooding caused high injection pressure, fast breakthrough and a rapid decrease in oil recovery. Therefore, adopting new technical means for enhanced oil recovery (EOR) in glutenite reservoirs is urgently needed.

Nanofluid flooding using silica nanoparticles (SNPs) has attracted worldwide attention as a promising technology for EOR. SNPs are readily available and relatively inexpensive with minimal environmental safety concerns (Afekare et al., 2021). Their small size of less than 100 nm allows them to easily pass through the pores of tight rocks (Zhang et al., 2021; Miyasaka et al., 2023). The EOR mechanisms using SNPs mainly include disjoining pressure, wettability alternation, interfacial tension (IFT) reduction, viscosity adjustment and pore channel plugging reduction (Nikolov et al., 2010; Hemmat Esfe and Esfandeh, 2020; Nasr et al., 2021; Goharzadeh et al., 2023). Kondiparty et al. (2011) observed the disjoining pressure induced by the self-structuring phenomenon of SNPs

in the confined three-phase contact region, which separates the oil from the rock surface through optical interferometry methods. As the oil is stripped from the rock surface, the nanofluid spreads on the rock surface, and the wettability of the rock also transforms from oil-wet to water-wet (Eltoum et al., 2021). The presence of SNPs at the interfacial layers also leads to IFT reduction (Joonaki and Ghanaatian, 2014). Both wettability alternation and IFT reduction are favorable for decreasing capillary forces that allow oil droplets to be squeezed from pores, thus resulting in residual oil production (Cheraghian and Hendraningrat, 2016). The synergy of sodium dodecyl sulfate (SDS) surfactant and nanoparticles also performs well in the EOR and improves the nanofluid by reducing nanoparticle agglomeration (Kumar et al., 2020). Xu et al. (2023) conducted huff-n-puff experiments using nanofluid and pure water. They showed that compared to pure water, nanofluids could effectively strip oil from small pores, clearly improving oil recovery.

Nanofluid technology has great potential to improve oil production in the Baikouquan glutenite reservoir. However, Baikouquan tight glutenite is characterized by complex mineral compositions and pore structures. The modification effects of the nanofluid and its compositions on the rock surface with complex mineral composition are worth further study. Moreover, compared to simple aggregates (Lv and Wang, 2015; Zhao and Wen, 2017), complex mineral pore structures lead to the generation of dominant channels, thus complicating the flow behavior of nanofluid flooding and affecting oil recovery using nanofluids. There is ambiguity about the effects of nanofluids on wettability change, IFT reduction and the pore-scale flow behavior in tight glutenite. Therefore, it is urgent
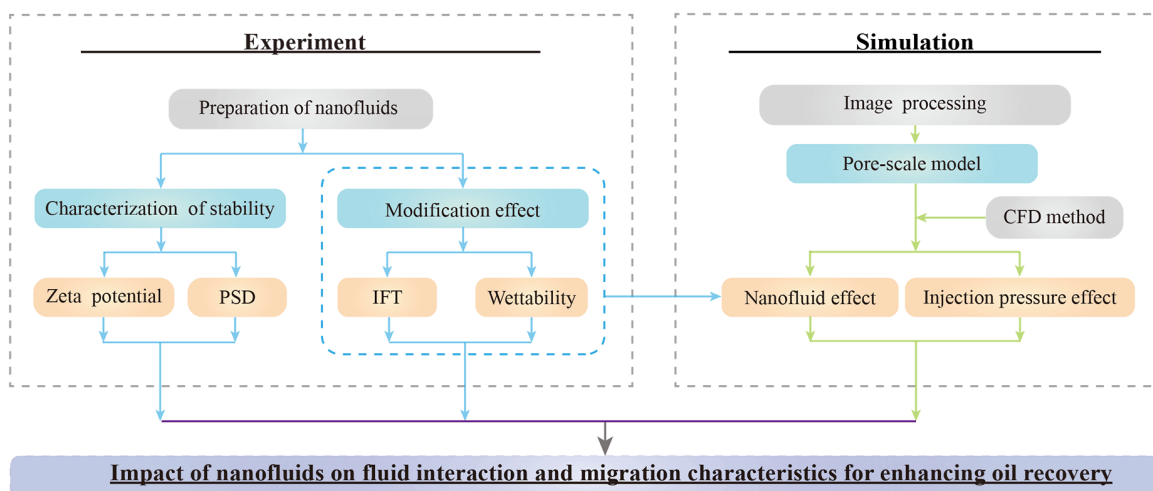
Fig. 2. Flowchart of the research methodology.

to carry out relevant research on the modification effect and EOR mechanism in tight glutenite using nanofluids, which can provide certain guidance for subsequent field applications.

This study aims to provide a comprehensive understanding of the EOR mechanisms using nanofluids at the pore scale. First, six groups of nanofluids with different concentrations were prepared and characterized by measuring the zeta potential and particle size distribution (PSD). Second, the modification effects of nanofluids on IFT and tight glutenite wettability were also examined. Finally, combining the experimental data with a pore-scale model based on the pore characteristics derived from scanning electron microscopy (SEM) images of tight glutenite samples, a computational fluid dynamics method was adopted to understand the process of multiphase flow and the effects of nanofluids and injection pressure on EOR in glutenite samples. Fig. 2 presents the details of the research methodology. This work will deepen our knowledge of EOR mechanisms using nanofluids at the pore scale and be instructive for the exploitation of the Baikouquan Formation reservoir.

2. Methodology

2.1 Materials

Hydrophilic N20 SNPs were obtained from Wacker Chemie AG, Germany, with a purity of 99.8%. Their surface area, dry density and average single particle size are 200 m^2/g, 2.2 g/m^3 and 12 nm, respectively. SDS (CAS# 151-21-3) was supplied by Aladdin, China, with a purity of 99.0%. Six groups of nanofluids (NF1-NF6) were prepared by dispersing different concentrations of SNPs and SDS into pure water according to the proportions shown in Table 1. The mixtures were stirred for 30 minutes until there was no obvious flocculent precipitation and then placed into an ultrasonic oscillator for two hours to fully disperse the mixtures and prevent nanoparticle agglomeration. Finally, the nanofluids were left to rest at room temperature for 48 hours to ensure that no agglomeration occurred.

Table 1. The compositions of the nanofluids.

Compositions	NF1	NF2	NF3	NF4	NF5	NF6
SNPs (wt%)	0.01	0.05	0.10	0.05	0.05	0.05
SDS (wt%)	0	0	0	0.01	0.05	0.10

2.2 Characterization and performance measurements of nanofluids

2.2.1 Zeta potential and PSD measurement

A NanoBrook 90plus PALS (phase angle light scattering) system (Brookhaven, USA) was used to measure the zeta potential of the nanofluids. With this approach, laser light is passed through the nanoparticle solution, which is subjected to varying electric fields; the frequency shift due to the Doppler effect is measured and then related to the zeta potential using the Hückel approximation. For these measurements, 1.3 mL of the nanofluid was placed into the sample cell where a clean electrode was inserted and completely immersed into the nanofluid. After the electrode is connected, the sample cell is placed into the sample tank of the instrument. Subsequently, the test temperature was set to 25 °C, the Hückel model was chosen as the potential mode, and the time interval was set to 60 seconds.

The same apparatus was used to measure the PSD of the nanofluids based on the principle of light intensity fluctuations caused by Brownian motion of particles in suspension. The fluctuations can be processed by digital correlator technology, from which the particle size and its distribution can be obtained. Using a similar approach to the zeta potential measurement, 1.3 mL of the nanofluid was placed into a transparent sample cell, which was placed into the sample tank of the instrument. Prior to the measurement, the temperature was set to 25 °C, and the scattering angle was set to 90°. The single measurement time and equilibrium time were set as 180 seconds and 20 minutes, respectively. The shape factor was set to uniform sphericity, and then the PSD of the internal

nanofluid could be obtained automatically.

2.2.2 IFT and contact angle measurement

A Dataphysics OCA20 system (optical contact angle, Germany) was used to measure the IFT via a pendant-drop method. When a droplet is suspended statically at the orifice of a capillary tube, its shape is primarily determined by the balance of gravity and surface tension. By modeling the droplet shape, the IFT can be calculated. Using an autosampler, either water or samples of NF1-NF6 nanofluids were slowly dropped from the probe into a glass tank filled with mineral oil. The droplet shape was recorded by the camera, and the coordinates of the hanging droplet contour were obtained by capturing, digitizing and processing the image of the hanging droplet. Using these data, the IFT was calculated by the SCA20 software module.

The contact angle was also measured using the Dataphysics OCA20 system based on a sessile drop method, which can automatically recognize the three-phase contact contour of the droplet and calculate the contact angle based on the tangent line between the contour line and baseline. For these measurements, a tight conglomerate rock sample collected from the Baikouquan Formation was selected and ground to powder with a grinding machine. The mineral powder was sieved to a diameter of less than 75 μm and mixed with water to a viscous state. Then, this mixture was evenly spread onto the surface of a quartz plate and placed into a drying oven at 60 °C for two days. Following this, the pretreated quartz plate was placed upside down in the quartz ark containing water or the NF1-NF6 nanofluids. An oil droplet was introduced at the surface, and the three-phase contact angle was observed and recorded.

2.3 Numerical simulation process

2.3.1 Governing equations

Computational fluid dynamics method was adopted to research the effects of nanofluids and injection pressure on EOR processes within the pore space of a simulated Baikouquan tight glutenite. The incompressible Navier-Stokes equation was used to describe the two-phase flow processes of water/-nanofluids and oil (Chauhan et al., 2021):

$$\nabla \cdot \vec{u} = 0 \tag{1}$$

$$\frac{\partial}{\partial t} \rho \vec{u} + \rho \nabla \cdot (\vec{u}\vec{u}) = -\nabla p + \mu \nabla \cdot \left(\nabla \vec{u} + \nabla \vec{u}^T\right) + \vec{F} + \rho \vec{g} \tag{2}$$

where $\vec{u}$ is the velocity vector, t is the time, ρ is the density of the fluid, p is the static pressure, μ is viscosity, $\vec{u}^T$ is the matrix transpose of $\vec{u}$, $\vec{F}$ is a general body force and $\vec{g}$ is the gravitational acceleration, which is negligible in this pore-scale simulation.

The Eulerian-Eulerian volume of fluid method was adopted to obtain the solution of the incompressible Navier-Stokes equations for two phases of water/nanofluids and oil. The listed volume fraction equation is used for tracking the interface between two phases (Zhao et al., 2019):

$$\frac{\partial (\alpha_i \rho_i)}{\partial t} + \nabla \cdot (\alpha_i \rho_i \vec{u}) = \rho_i S_{\alpha_i} + \sum_{j=1}^{n} \left(\dot{m}_{ji} - \dot{m}_{ij}\right) \tag{3}$$

where α_i is the volume fraction of phase i, S_{α_i} is the source term of phase i, and $\dot{m}_{ji}$ and $\dot{m}_{ij}$ are the mass transfer from each other between phase i and phase j, respectively. Based on the above assumptions, $\dot{m}_{ji}$ and $\dot{m}_{ij}$ were taken as zero owing to the no mass-transfer assumption between water/nanofluids and the oil phase. Here, the interface between two phases was tracked based on the volume fraction α_i in the cell, and α_i is defined as follows:

1) $\alpha_i = 0$: the cell does not contain the fluid;
2) $\alpha_i = 1$: the cell only contains the fluid;
3) $0 < \alpha_i < 1$: the cell only contains the fluid interface;
4) $\sum_{p=1}^{n} \alpha_p = 1$: the cell must be filled with a single-phase fluid or a combination.

The fluid properties in the interface cell are different from those of a single-phase fluid, which are obtained by the following equations (Gharibshahi et al., 2015):

$$\rho = \sum \alpha_i \rho_i \tag{4}$$

$$\mu = \sum \alpha_i \mu_i \tag{5}$$

The continuum surface force model was employed to calculate the curvature of the interface and volume surface tension. The equations used to obtain the volume surface tension are listed below:

$$\vec{F} = \sigma k \nabla \alpha_i \tag{6}$$

$$k = \nabla \cdot \vec{n} \tag{7}$$

where σ is the IFT, k is the curvature, and $\vec{n}$ is the unit normal vector of the interface. Specifically, $\vec{n}$ is influenced by the contact angle if the cell is located near the wall (Chauhan et al., 2021):

$$\vec{n} = \vec{n_w} \cos \theta_w + \vec{t_w} \sin \theta_w \tag{8}$$

where $\vec{n_w}$ and $\vec{t_w}$ are the unit vectors normal and tangential to the wall, respectively, and θ_w is the fluid contact angle.

2.3.2 Pore-scale model construction

As shown in Fig. 3(a), the pore characteristics of Baikouquan tight glutenite were scanned by SEM. The light gray part of the SEM image represents the rock matrix, and the dark gray part represents the pores where water or nanofluids would displace oil. To facilitate EOR numerical simulation, the pores were extracted from the SEM image as displacement channels, and a two dimensional pore-scale model was constructed (Fig. 3(b)). The length and height of the model are 25.4 and 14.96 μm, respectively, which are consistent with the shape and size of the pores in the SEM results. The left edge of the model was set to the constant-pressure inlet for injecting water or nanofluids into the model, and the right edge of the model was designed with a constant-pressure outlet where oil would flow out. The boundary condition for the pore wall was stationary and no-slip. To reproduce the oil displacement
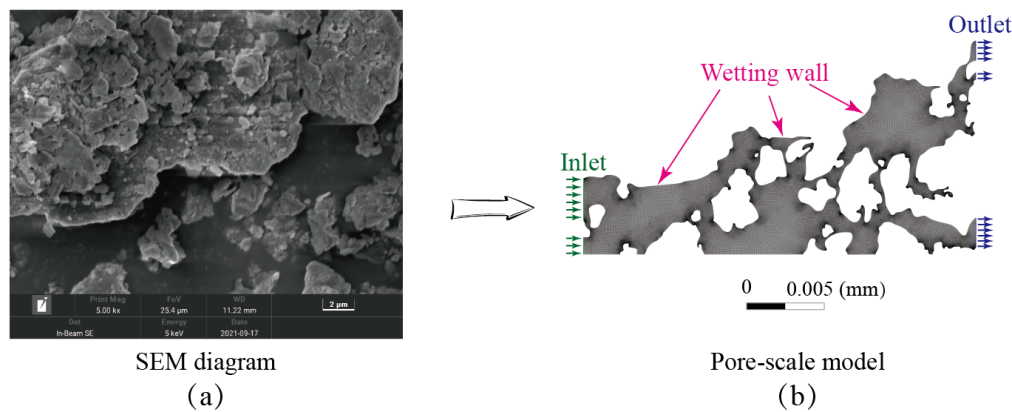
SEM diagram
(a)

Pore-scale model
(b)

Fig. 3. The process of establishing a pore-scale model: (a) raw SEM image and (b) pore-scale model.

processes using water and different nanofluids (NF1-NF6), different contact angle values and IFT results obtained from experiments were given in different fluid flooding processes. As only small amounts of SNPs and SDS were added (Table 1), the density and dynamic viscosity of all nanofluids (NF1-NF6) were set to be the same as water, which were 998.2 kg/m^3 and 1.003 mPa·s, respectively. In the initial stage, the model was filled with oil, with a density of 879 kg/m^3 and dynamic viscosity of 6.37 mPa·s. The model was discretized into fine structured meshes by the Multizone Quad/Tri method with 128852 computational cells and 133274 nodes to ensure that the results were independent of the mesh resolution (Fig. 3(b)).

A total of 14 cases were simulated to investigate the effects of nanofluid compositions and injection pressure on EOR in Baikouquan tight glutenite. More specifically, water and NF1-NF6 were injected into the model with a total injection volume of 10 pore volume (PV) under injection pressure differences (IPDs) of 1 and 5 MPa.

3. Results and discussion

3.1 Zeta potential and PSD results of nanofluids

The zeta potential is an important indicator of nanoparticle stability that reflects the interparticle electrostatic repulsive force. Typically, a nanofluid system is considered stable when its zeta potential is either higher than +30 mV or lower than -30 mV (Chakraborty and Panigrahi, 2020). A larger absolute value of the zeta potential usually demonstrates a more uniform and stable particle dispersion. Fig. 4(a) presents the measured zeta potentials of the six groups of nanofluids, all of which were less than -30 mV, indicating quite stable nanofluid systems. The average zeta potentials of the NF1, NF2 and NF3 nanofluids were -33.18, -43.30 and -45.36 mV, respectively. This suggests that the nanofluid system became more stable with increasing hydrophilic SNPs. Meanwhile, the average zeta potentials of NF4, NF5, and NF6 were reduced to -57.35, -60.33 and -56.56 mV, indicating that SDS is also favorable for stabilizing the nanofluid system. The SNPs are negatively charged, and their surface charge increases with increasing SNP concentration. After anionic surfactant SDS

was added into silica nanofluid systems, the negatively charged dodecyl sulfate anion (DS$^-$) dissociated from SDS would adsorb on the surface of SNPs (Pan et al., 2010; Muhamad et al., 2015), leading to a further decrease in the zeta potential.

Fig. 4(b) displays the PSDs of the six groups of nanofluids. The PSDs of NF1-NF6 were well dispersed and uniform, which further confirmed the stability of all systems mentioned above. The average nanoparticle sizes were 691.61, 488.86 and 432.31 nm for NF1-NF3, respectively. After adding SDS, the average nanoparticle sizes further decreased to 376.82, 337.32, and 334.51 nm for NF4-NF6, respectively. As mentioned before, the diameter of the SNPs is 12 nm in the dried and solid-states. After the SNPs were dispersed into water, hydrolysis and condensation processes occurred, causing some SNPs to bind together. Therefore, the average nanoparticle size in the nanofluid is much larger than the diameter of a single nanoparticle. With the increase of SNP concentration, the average nanoparticle size decreased. This is because the higher the absolute value of the zeta potential is, the greater the electrostatic repulsion exists among SNPs and the more dispersed the SNPs are. Meanwhile, the average nanoparticle size also decreased with increasing SDS concentration at a given SNP concentration of 0.05 wt%. This is due to the negatively charged DS$^-$ dissociated by SDS bound to SNPs and effectively inhibiting the condensation process of SNPs. In addition, the smaller SNPs could provide larger surface areas for DS$^-$ to bind. The process is mutually reinforced.

3.2 Effect of nanofluids on IFT and wettability

Fig. 4(c) illustrates the IFT between oil and water/nanofluids, which quantifies the assembly of nanoparticles at the oil-water/nanofluid interface (Zhou et al., 2019). The IFT between the water and oil was 46.12 mN/m, while those between NF1-NF3 and oil were 39.9, 37.79 and 37.77 mN/m, presenting a reduction of 13.48%, 18.06% and 18.01% compared to water, respectively. This reduction can be attributed to the SNPs, which are located at the oil-water interfaces so that the friction between the two phases decreases (Moradi et al., 2015). Previous studies have also verified this statement via molecular dynamics simulations of the distribution of nanoparticles (Gysi and Stefánsson, 2012; Yu et al., 2022). After adding SDS, the
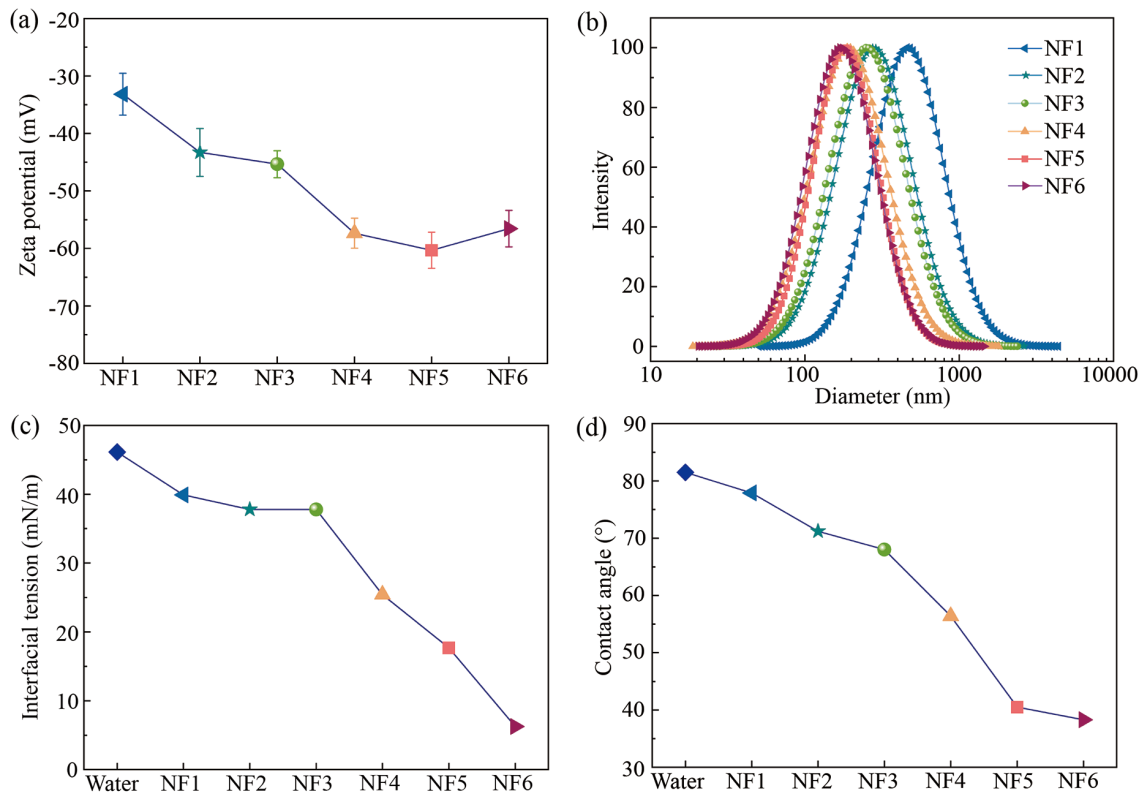
Fig. 4. The results of (a) zeta potential, (b) PSD, (c) IFT and (d) contact angle between the oil and water/nanofluids.

IFT between NF4-NF6 and oil decreased to 25.43, 17.68 and 6.26 mN/m, which presents a reduction of 44.86%, 61.67% and 86.43% compared to water, respectively. The synergy of SNPs and SDS exhibits a more pronounced effect on IFT reduction than individual SNPs. After SDS is added, the dissociated DS^- absorbs on the surface of the SNPs through hydrogen bonding between the hydroxyl groups of the SNPs and the hydrophobic tails of DS^-. The hydrophilic heads (the silica part) point toward the water phase, while the hydrophobic carbon chains (DS^-) enter the oil phase, resulting in a blurred water-oil interface (Saien and Bahrami, 2016; Mousavi et al., 2021). As a result, the interface becomes more miscible, and the IFT decreases further with increasing SDS concentration.

The contact angle is a fundamental parameter for evaluating the wettability of reservoir rock. The rock is considered intermediate-wet when the contact angle (θ) is between 70° and 110°. It is strongly water-wet when $\theta < 50°$ and weakly water-wet when $50° < \theta < 70°$. When θ ranges from 110°-130° and 130°-180°, the rock is considered weakly oil-wet and strongly oil-wet, respectively (Yekeen et al., 2020). Fig. 4(d) exhibits the results of the water/nanofluids-oil-rock three-phase contact angle. The contact angle for the water-oil-rock system was 81.5°, so the initial wettability of the reservoir was considered intermediate-wet. In the presence of SNPs, the contact angle was reduced to 77.9°, 71.2° and 68° for NF1-NF3, respectively. Thus, the wettability of the rock was shifted to weakly water-wet. After adding SDS, the contact angle was further reduced to 56.4°, 40.5° and

38.3° for NF4-NF6, respectively, indicating a conversion of the wettability of rock to strongly water-wet. The prepared nanofluids could obviously alter the reservoir wettability from neutral wetting to hydrophilic wetting, and the main reasons for this can be divided into two aspects. On the one hand, due to their high specific surface area, SNPs can easily adsorb on the rock surface, and the electrostatic repulsion between nanoparticles allows nanofluids to spread along the surface (Adil et al., 2020). Additionally, the driving pressure of the bulk liquid also helps the nanofluid spread along the surface (Hendraningrat et al., 2013). The adsorbed and deposited hydrophilic SNPs on the rock surface transform from a neutral-wet state to a water-wet state on the wettability of reservoir rock. On the other hand, the adsorbed SNPs at the solid-oil-nanofluid three-phase interface form a wedge film, and the confined nanoparticles in the three-phase contact region tend to form more ordered structures, generating an excess pressure (i.e., disjoining pressure) that points from the aqueous phase to the oil phase (Kondiparty et al., 2011; Li et al., 2018). The disjoining pressure overcomes the adhesion force of the rock surface and oil, causing the oil to peel off. Brownian motion and electrostatic repulsion between the nanoparticles provide energies for disjoining pressure (Almahfood and Bai, 2018). Furthermore, the effect of nanofluids on the wettability alteration of the rock surface is more profound after adding SDS. This is because the performance of SNPs as a wettability modifier can be greatly improved due to the adsorption of DS^- on their surfaces, generating a larger repulsive force and disjoining pressure. This corresponds with decreasing IFT, as
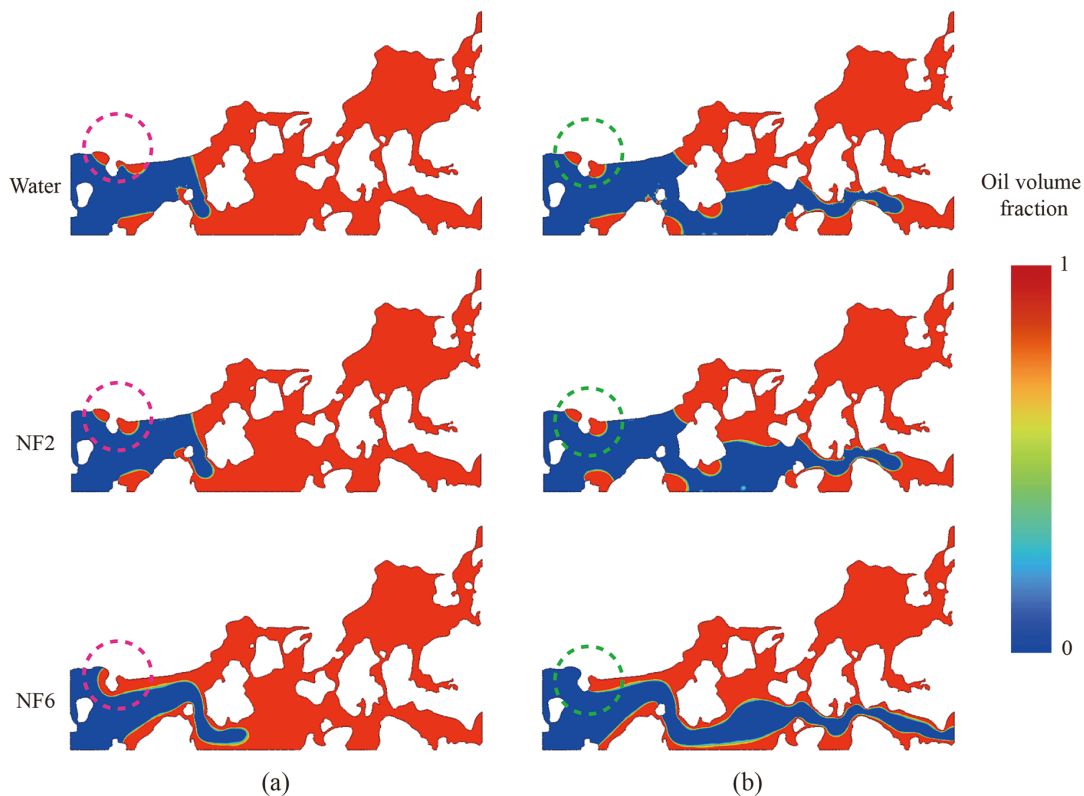
Fig. 5. The distributions of water/nanofluids and oil phases under injection volumes of (a) 0.2 PV and (b) 0.4 PV with an IPD of 1 MPa.

shown in Fig. 4(c), which means that the ability of oil to spread on oil decreases, resulting in a smaller contact angle.

3.3 Effect of nanofluids on displacement fluid migration characteristics

The simulation results show that the oil displacement processes using water/nanofluids could be divided into two stages: the initial channel establishment stage, i.e., the period in which the injected fluid did not flow out of the model outlet; and the channel expansion stage, i.e., the period in which the injected fluid did flow out of the outlet. In the presence of nanofluids, the migration behavior of the displacement fluid was altered due to the IFT reduction and wettability alternation. The volume fraction distributions of injection fluid (including water, NF2 and NF6) phase and oil phase under the injection volumes of 0.2 PV and 0.4 PV with the IPD of 1 MPa are displayed in Fig. 5.

In comparison to the water flooding process, the shapes of displacement fluid front were almost the same and the migration velocities of the displacement fluid front only slightly increased using NF2 flooding with the addition of SNPs. The possible reason is the weak effect of single SNPs on IFT reduction and wettability modification (Figs. 4(c) and 4(d)). During the NF6 flooding process, the shapes of the displacement fluid front were obviously sharper and the migration velocities of the displacement fluid front increased significantly with the addition of both SNPs and SDS. The

intersection angle between the migration front of NF6 and the pore wall were more curved compared with water and NF3 because of the wettability alternation (see purple circles), causing the relative dead oil in water and NF2 flooding to be movable (see green circles). Moreover, the NF6 broke through the pore model after 0.4 PV injection, while the water and NF2 did not reach the outlet when 0.4 PV was injected. This may be ascribed to the rapidly decreasing IFT with the synergistic effect of SNPs and SDS, resulting in a decrease in resistance of displacement fluid. The injection process before breakthrough can be considered to be the initial channel establishment stage.

After the breakthrough phenomenon occurred, the displacement fluids continued to be injected into the models. Fig. 6 displays the fluid distributions with injections of 4 PV and 10 PV under an IPD of 1 MPa. The continuously injected displacement fluids were divided into two parts. Some of the fluid flowed out of the model along the initial channel, while some of the fluid displaced the oil along the initial channel and expanded it. As the channel expanded, the nanofluid could enter some relative dead pores during water flooding processes and displace the oil (see purple circles and blanks). The role of nanofluids in EOR was subsequently reflected. This phenomenon is not so obvious in the process of NF2 flooding, which may be because NF2 causes little change in the IFT and reservoir wettability. However, the phenomenon was most remarkable during the NF6 flooding processes where the oil in the pores near the inlet was almost completely displaced.
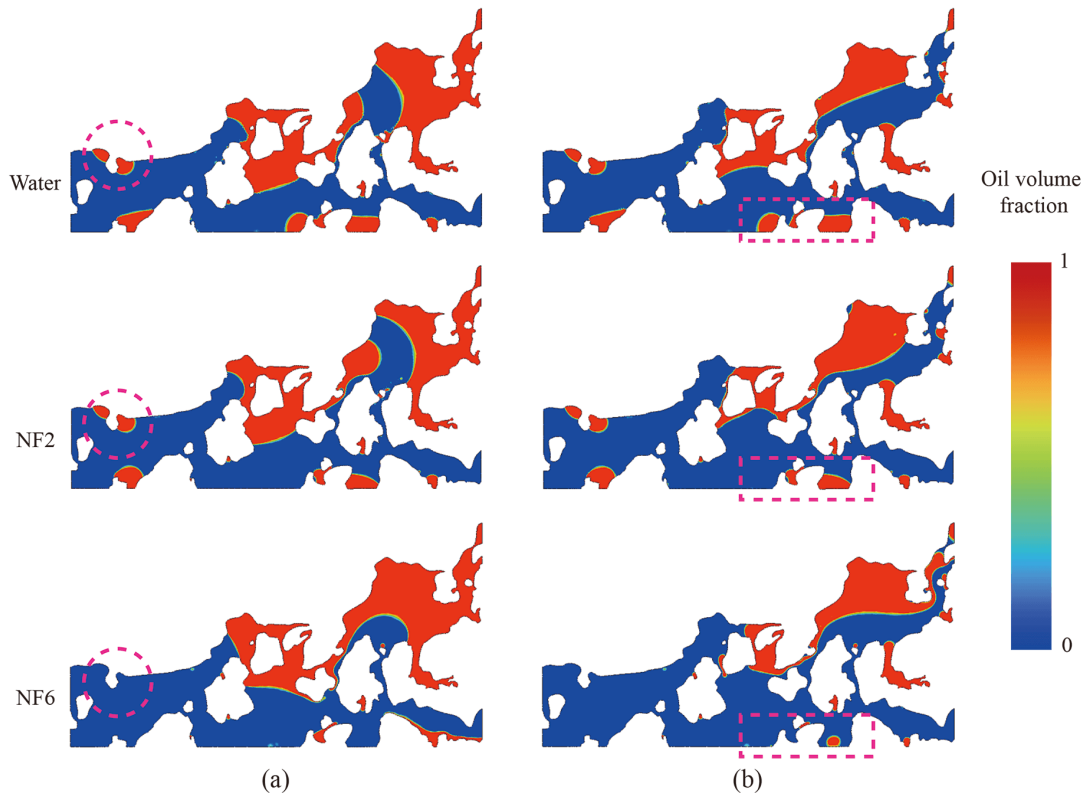
Fig. 6. The distributions of water/nanofluids and oil phases under injection volumes of (a) 4 PV and (b) 10 PV with an IPD of 1 MPa.

3.4 Effect of injection pressure on fluid behaviors

To reflect the influence of injection pressure on fluid behaviors, the displacement processes during the NF2, NF4 and NF6 are illustrated and shown in Figs. 7 and 8. The comparisons of fluid mobilization profile in the initial channel establishment stage with different IPDs of 1 and 5 MPa are displayed in Fig. 7. Under the same injection volume, the shapes of all nanofluid fronts with an IPD of 5 MPa were sharper than those with an IPD of 1 MPa. Meanwhile, the migration velocities of nanofluids were also faster with a higher IPD. Therefore, the nanofluids were more likely to break through the model under a higher IPD. Moreover, under an IPD of 5 MPa, the nanofluids with high velocity hardly contacted the pore surface and primarily displaced the oil in the middle of the pores (see the green circles). Therefore, the higher IPD had negative effects on EOR in the initial channel establishment stage due to its smaller sweep area. Fig. 8 shows the comparisons of fluid mobilization profiles under the injection of 8 PV nanofluids at different IPDs. In all cases, one part of continuously injected nanofluid flowed out of the model and another part displaced the residual oil along the initial channel and expanded it. The higher IPD played two roles during the displacement processes. On one hand, a higher IPD lead to the extraction of relative dead oil under lower IPD (see purple circles), resulting in higher oil recovery. On the other hand, the nanofluids exhibit sharper migration

fronts under a higher IPD (see green blanks), which lead to smaller sweep areas around the outlet.

Therefore, the effect of IPD on oil recovery is a complex process and varies with injection volume of nanofluids. In the initial channel establishment stage, nanofluids have larger sweep areas with a lower IPD than that with a higher IPD with the same amount of injected nanofluids. In the channel expansion stage, the higher IPD could show an EOR effect near the inlet as the nanofluid could strip the oil in relative dead pores with a lower IPD. With continuous injection, the IPD on EOR using nanofluids became more distinct.

3.5 Effect of nanofluids and injection pressure on oil recovery efficiency

As mentioned previously, the displacement process can be divided into two stages: the initial channel establishment stage and the channel expansion stage. The oil recoveries of all cases in different stages are shown in Fig. 9. When the breakthrough occurred under an IPD of 1 MPa, the oil recoveries were 36.67%, 36.27%, 36.13%, 35.78%, 33.53%, 31.70% and 28.24% for water and NF1-NF6, respectively. It is evident that nanofluids cannot improve oil recovery efficiencies in the initial channel establishment stages. This is due to the gradual enhancement of pore surface wettability alternation and IFT reduction effects (Figs. 4(c) and 4(d)) with increasing SNPs and SDS concentrations, which leads to sharper displacement fluid fronts and faster migration rates
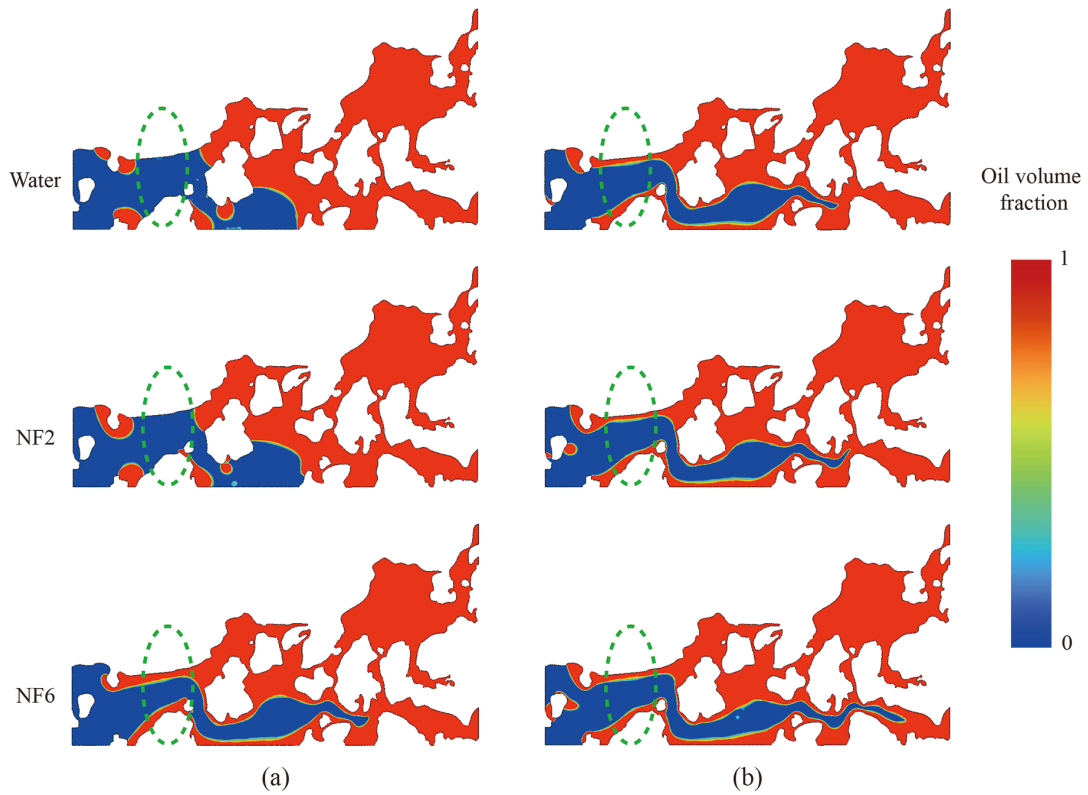
Fig. 7. Comparisons of fluid mobilization profiles under injection volumes of 0.3 PV at IPDs of (a) 1 MPa and (b) 5 MPa.
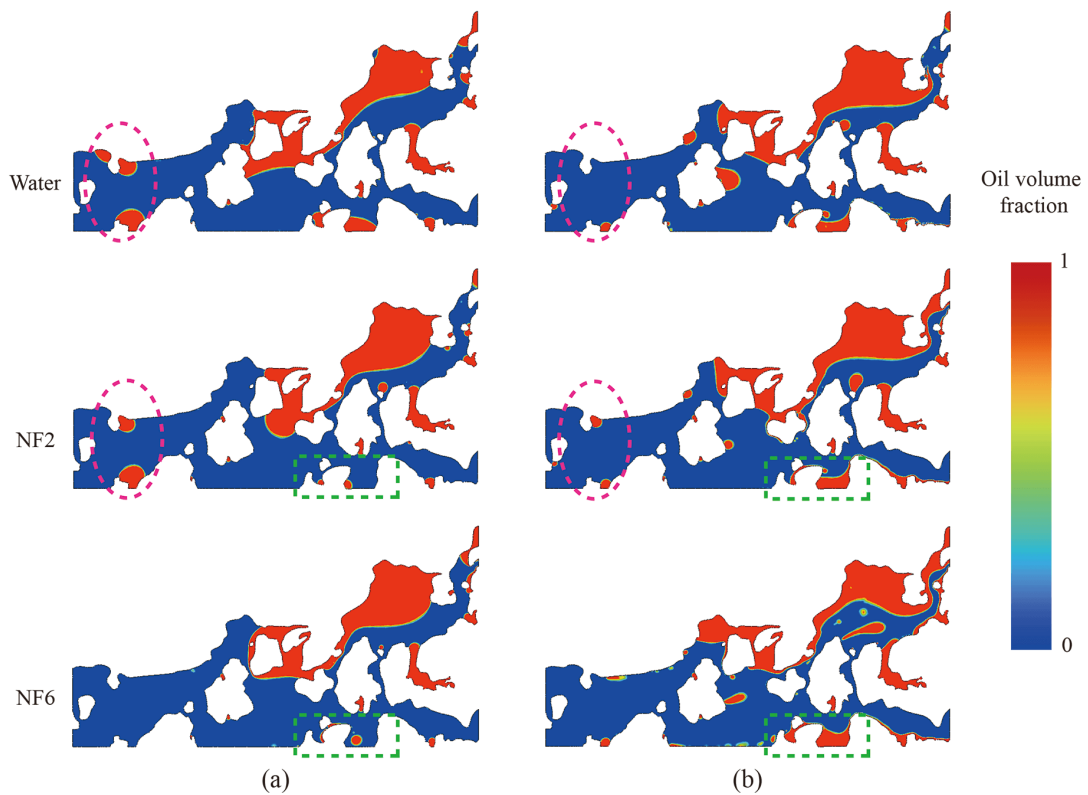

Fig. 8. Comparisons of fluid mobilization profiles under injection volumes of 8 PV at IPDs of (a) 1 MPa and (b) 5 MPa.
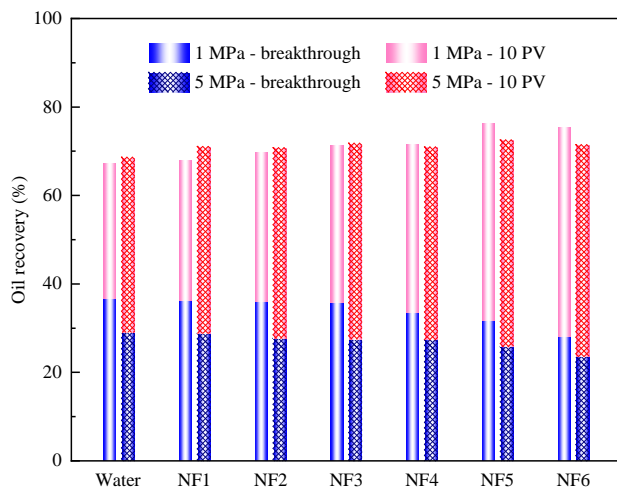
Fig. 9. Oil recoveries during the displacement processes.

during the flooding processes (Fig. 5). Thus, before the breakthrough occurred, the swept areas of the NF1-NF6 nanofluids gradually decreased contributing to the progressive reduction of oil recovery. However, during the channel expansion stages, nanofluids with a strong modification effect were more likely to displace oil along the channels and even displace the oil existing in the pores, which were the dead pores for the water flooding process (Fig. 6). After 10 PV of displacement fluids was injected into the model with an IPD of 1 MPa, the oil recoveries were 67.43%, 68.23%, 69.9%, 71.47%, 71.85%, 76.58% and 75.57% for the water and NF1-NF6 nanofluids flooding processes, respectively. The nanofluids showed a very significant oil displacement effect and great ability to improve oil recovery.

As shown in Figs. 7 and 8, the IPD has a complex effect on the fluid behaviors in oil displacement processes; therefore, the influence of IPD on oil recovery efficiency also differs. Prior to the breakthrough occurring, as the higher IPD brought sharper migration fronts and smaller sweep areas of displacement fluids (Fig. 7), the higher IPD even had negative effects on EOR with the oil recovery efficiencies of 29.09%, 28.82%, 27.69%, 27.56%, 27.38%, 25.78% and 23.58% for water and NF1-NF6, respectively. After 10 PV displacement fluids were injected, the NF1-NF3 showed higher oil recovery efficiencies under higher IPD, which were 71.08%, 70.80% and 71.85%, respectively. However, the situations for NF4-NF6 showed opposite trends; that is, the oil recovery efficiencies were 71.00%, 72.57% and 71.48%, respectively. This is because the higher IPD makes the original sharp migration fronts of NF4-NF6 sharper.

4. Summary and conclusions

In this paper, six groups of nanofluids were prepared with varying concentrations of SNPs and SDS. The zeta potential and PSD were measured to characterize the stability of the nanofluids. The effects of the nanofluids on IFT reduction and reservoir wettability alteration of the Baikouquan Formation tight glutenite were also examined. Based on the experimental results, the computational fluid dynamics method was used to

further investigate the effects of nanofluids and injection pressure on EOR in a pore-scale model. The following conclusions can be generally drawn:

1) The zeta potentials of the six groups of nanofluids were all less than -30 mV, and their PSDs were well dispersed and uniform, which indicated that the prepared nanofluid systems were quite stable.

2) The nanofluids effectively reduced the IFT and converted the wettability of tight glutenite from intermediate-wet to strongly water-wet. Furthermore, the modification effect was more pronounced with increasing concentrations of SNPs and SDS.

3) The displacement processes could be divided into two stages: the initial channel establishment stage and the channel expansion stage. At the initial channel establishment stage, the nanofluids did not show an EOR effect and even had negative effects. Obvious EOR effects emerged in the channel expansion stage mainly because the nanofluids could displace oil in the relative dead pores during water flooding.

4) The higher IPD led to the extraction of relative dead oil under lower IPD and facilitated higher oil recovery, while it also resulted in a smaller sweep area near the outlet and reduced the oil recovery during nanofluid flooding processes. The influence of injection pressure on the overall oil recovery efficiency of the model needs further study.

5) The case in which 10 PV of NF5 is injected under an IPD of 1 MPa has the highest oil recovery efficiency of 76.58%. Microfluidic experiments and core-scale experiments are our next step for further confirming the simulation results.

Conflict of interest

The authors declare no competing interest.

References

Adil, M., Zaid, H. M., Raza, F., et al. Experimental evaluation of oil recovery mechanism using a variety of surface-modified silica nanoparticles: Role of in-situ surface-modification in oil-wet system. PLoS ONE, 2020, 15(7): 0236837.

Afekare, D., Garno, J., Rao, D. Enhancing oil recovery using silica nanoparticles: Nanoscale wettability alteration effects and implications for shale oil recovery. Journal of Petroleum Science and Engineering, 2021, 203: 108897.

Almahfood, M., Bai, B. The synergistic effects of

nanoparticle-surfactant nanofluids in EOR applications. Journal of Petroleum Science and Engineering, 2018, 171: 196-210.

Bera, A., Vij, R. K., Shah, S. Impact of newly implemented enhanced oil and gas recovery screening policy on current oil production and future energy supply in India. Journal of Petroleum Science and Engineering, 2021, 207: 109196.

Chakraborty, S., Panigrahi, P. K. Stability of nanofluid: A review. Applied Thermal Engineering, 2020, 174: 115259.

Chauhan, A., Salehi, F., Jalalifar, S., et al. Two-phase modelling of the effects of pore-throat geometry on enhanced oil recovery. Applied Nanoscience, 2021, 13(1): 453-464.

Cheraghian, G., Hendraningrat, L. A review on applications of nanotechnology in the enhanced oil recovery part B: Effects of nanoparticles on flooding. International Nano Letters, 2016, 6(1): 1-10.

Chowdhury, S., Shrivastava, S., Kakati, A., et al. Comprehensive review on the role of surfactants in the chemical enhanced oil recovery process. Industrial & Engineering Chemistry Research, 2022, 61(1): 21-64.

Eltoum, H., Yang, Y. L., Hou, J. R. The effect of nanoparticles on reservoir wettability alteration: A critical review. Petroleum Science, 2021, 18(1): 136-153.

Gharibshahi, R., Jafari, A., Haghtalab, A., et al. Application of CFD to evaluate the pore morphology effect on nanofluid flooding for enhanced oil recovery. RSC Advances, 2015, 5(37): 28938-28949.

Goharzadeh, A., Fatt, Y. Y., Sangwai, J. S. Effect of TiO_2-SiO_2 hybrid nanofluids on enhanced oil recovery process under different wettability conditions. Capillarity, 2023, 8(1): 1-10.

Gysi, A. P., Stefánsson, A. CO_2-water-basalt interaction. Low temperature experiments and implications for CO_2 sequestration into basalts. Geochimica et Cosmochimica Acta, 2012, 81: 129-152.

Hemmat Esfe, M., Esfandeh, S. 3D numerical simulation of the enhanced oil recovery process using nanoscale colloidal solution flooding. Journal of Molecular Liquids, 2020, 301: 112094.

Hendraningrat, L., Li, S. D., Torster, O. A coreflood investigation of nanofluid enhanced oil recovery. Journal of Petroleum Science and Engineering, 2013, 111: 128-138.

Joonaki, E., Ghanaatian, S. The application of nanofluids for enhanced oil recovery: Effects on interfacial tension and coreflooding process. Petroleum Science and Technology, 2014, 32(21): 2599-2607.

Kalam, S., Abu-Khamsin, S. A., Kamal, M. S., et al. A review on surfactant retention on rocks: Mechanisms, measurements, and influencing factors. Fuel, 2021, 293: 120459.

Kondiparty, K., Nikolov, A., Wu, S., et al. Wetting and spreading of nanofluids on solid surfaces driven by the structural disjoining pressure: Statics analysis and experiments. Langmuir, 2011, 27(7): 3324-3335.

Kumar, R. S., Chaturvedi, K. R., Iglauer, S., et al. Impact of anionic surfactant on stability, viscoelastic moduli, and oil recovery of silica nanofluid in saline environment.

Journal of Petroleum Science and Engineering, 2020, 195: 107634.

Li, Y., Dai, C., Zhou, H., et al. Investigation of spontaneous imbibition by using a surfactant-free active silica water-based nanofluid for enhanced oil recovery. Energy & Fuels, 2018, 32(1): 287-293.

Lv, M., Wang, S. Pore-scale modeling of water/oil two-phase flow in hot water flooding for enhanced oil recovery. RSC Advances, 2015, 5(104): 85373-85382.

Miyasaka, K., Imai, Y., Tajima, K. Preparation of oil-in-water and water-in-oil emulsions with the same composition using hydrophilic nanoparticles by three-phase emulsification. Colloids and Surfaces A: Physicochemical and Engineering Aspects, 2023, 670: 131598.

Mmbuji, A., Cao, R., Zhu, Z., et al. A comprehensive review of recent advances on surfactant architectures and their applications for unconventional reservoirs. Journal of Petroleum Science and Engineering, 2021, 206: 109025.

Moradi, B., Pourafshary, P., Jalali, F., et al. Experimental study of water-based nanofluid alternating gas injection as a novel enhanced oil-recovery method in oil-wet carbonate reservoirs. Journal of Natural Gas Science and Engineering, 2015, 27: 64-73.

Mousavi, S. P., Hemmati-Sarapardeh, A., Norouzi-Apourvari, S., et al. Toward mechanistic understanding of wettability alteration in calcite and dolomite rocks: The effects of resin, asphaltene, anionic surfactant, and hydrophilic nano particles. Journal of Molecular Liquids, 2021, 321: 114672.

Muhamad, M. S., Salim, M. R., Lau, W. J. Surface modification of SiO_2 nanoparticles and its impact on the properties of PES-based hollow fiber membrane. RSC Advances, 2015, 5(72): 58644-58654.

Nasr, M. S., Esmaeilnezhad, E., Choi, H. J. Effect of silicon-based nanoparticles on enhanced oil recovery: Review. Journal of the Taiwan Institution of Chemical Engineers, 2021, 122: 241-259.

Nikolov, A., Kondiparty, K., Wasan, D. Nanoparticle self-structuring in a nanofluid film spreading on a solid surface. Langmuir, 2010, 26(11): 7665-7670.

Pan, Y., Lu, X. C., Pan, G. S., et al. Performance of sodium dodecyl sulfate in slurry with glycine and hydrogen peroxide for copper-chemical mechanical polishing. Journal of the Electrochemical Society, 2010, 157(12): 1082-1087.

Rashidi, M., Kalantariasl, A., Saboori, R., et al. Performance of environmental friendly water-based calcium carbonate nanofluid as enhanced recovery agent for sandstone oil reservoirs. Journal of Petroleum Science and Engineering, 2021, 196: 107644.

Saien, J., Bahrami, M. Understanding the effect of different size silica nanoparticles and SDS surfactant mixtures on interfacial tension of n-hexane-water. Journal of Molecular Liquids, 2016, 224: 158-164.

Sidiq, H., Abdulsalam, V., Nabaz, Z. Reservoir simulation study of enhanced oil recovery by sequential polymer flooding method. Advances in Geo-Energy Research, 2019, 3(2): 115-121.

Wang, Y., Fan, D., Dong, S., et al. Domestic and international oil & gas resources situation analysis and outlook in 2022. China Mining, 2023, 32(1): 16-22. (in Chinese)

Xu, L., Li, Q., Myers, M., et al. Investigation of the enhanced oil recovery mechanism of CO_2 synergistically with nanofluid in tight glutenite. Energy, 2023, 273: 127275.

Yekeen, N., Padmanabhan, E., Sevoo, T. A. L., et al. Wettability of rock/CO_2/brine systems: A critical review of influencing parameters and recent advances. Journal of Industrial and Engineering Chemistry, 2020, 88: 1-28.

Yu, T., Li, Q., Hu, H., et al. Molecular dynamics simulation of the interfacial wetting behavior of brine/sandstone with different salinities. Colloids and Surfaces A: Physicochemical and Engineering Aspects, 2022, 632: 127807.

Zhang, C. J., Jin, X., Tao, J. P., et al. Comparison of nanomaterials for enhanced oil recovery in tight sandstone reservoir. Frontiers in Earth Science, 2021, 9: 746071.

Zhao, J., Wen, D. Pore-scale simulation of wettability and interfacial tension effects on flooding process for enhanced oil recovery. RSC Advances, 2017, 7(66): 41391-41398.

Zhao, J., Yao, G., Wen, D. Pore-scale simulation of water/oil displacement in a water-wet channel. Frontiers of Chemical Science and Engineering, 2019, 13(4): 803-814.

Zhou, H., Dai, C., Zhang, Q., et al. Interfacial rheology of novel functional silica nanoparticles adsorbed layers at oil-water interface and correlation with pickering emulsion stability. Journal of Molecular Liquids, 2019, 293: 111500.